Cartography of tomato pericarp cellular morphology at the fruit scale

David Legland, Marie Francoise Devaux, Brigitte Bouchet, Fabienne Guillon, Marc Lahaye

Cartography of tomato pericarp cellular morphology at the fruit scale

D. Legland[a,b,c,d], M.-F. Devaux[e], B. Bouchet[e], F. Guillon[e], M. Lahaye[e]

[a]*INRA, UMR782 Food Process Engineering and Microbiology, 78850 Thiverval-Grignon, France*
[b]*AgroParisTech, UMR782 Food Process Engineering and Microbiology, 78850 Thiverval-Grignon, France*
[c]*INRA, UMR 1318 Institut Jean-Pierre Bourgin, 78026 Versailles, France*
[d]*AgroParisTech, Institut Jean-Pierre Bourgin, 78026 Versailles, France*
[e]*INRA, UR1268 Biopolymers – Interactions and Assemblies, 44300 Nantes, France*

ABSTRACT

Consumer perception and industrial processing of fleshy fruits greatly depend on the morphology and spatial organization of cells within the tissues. To study the relations between the structure and the mechanical properties of fleshy fruits, it is necessary to quantify their cellular morphology. A generic approach is proposed to build cartographies of cellular morphology at the fruit scale, depicting regions corresponding to different cell morphologies. The approach is based on sampling the whole fruit at known positions, imaging and quantifying the local cellular morphology, pooling measurements to take into account the biological variability and projecting results in a 3D model of the whole fruit. The result is a synthetic representation of cell morphology variations within the whole fruit. Tomato pericarp was used as a model for fleshy fruits. Two different scales were investigated through 3D imaging using confocal microscopy, and macroscopy imaging of pericarp slices. The morphology of the tomato pericarp was assessed (1) from 3D microscopy images through stereological estimation of cell wall surface area and (2) from greyscale granulometry computed with mathematical morphology. Spatial heterogeneity within pericarp was described by measuring the morphology for different regions of interest within the whole fruit and for each characterisation method. This resulted in cartography of the cellular structure at the scale of the fruit; either by cell wall surface area estimate or by grey level mean size. Both methods presented complementary results, and made it possible to compare results obtained at different scales.

1 Introduction

The cell morphology of fleshy fruit is largely investigated in relation to fruit shape and size, mechanical properties or consumer perception. Many properties are measured at a macroscopic scale, e.g., mechanical tests on tissues, sensory or chemical analyses, etc. (Schotsmans et al., 2004, Ho et al., 2010). On the contrary, cell morphology is usually investigated through microscopy. These differences in scale make it difficult to establish relationships between cell morphology and fruit properties.

Fruit cells can be observed using microscopy with a good resolution and 3D images of fresh fruit tissues can easily be obtained (Gray et al., 1999; Legland et al., 2010, Pieczywek and Zdunek, 2012). A potential limitation is the size of the field of view that may be small compared to the typical size of a fruit cell. Macroscopy is an alternative to microscopy that allows the observation of a large area of plant tissue within a single image (Cheniclet et al., 2005; Devaux et al., 2008).

The variability of cell morphology at the fruit scale is largely unknown. It presents both a huge variability and a high level of organisation. Cell morphology depends on the tissue and on its location within the tissue, e.g., distance from the epidermis, pedicel or vascular bundles (Cheniclet et al., 2005; Devaux et al., 2008; Mebatsion et al., 2008). The description of this heterogeneity is usually investigated through the characterisation of a reduced number of clearly identified tissues or specific regions.

This study presents a generic approach to quantitatively describe cell morphology at the scale of the whole fruit, depicting regions corresponding to different cell morphologies. The approach is based on: (1) sampling the whole fruit at known positions; (2) imaging and quantifying local cell morphology; (3) pooling measurements to take biological variability into account and (4) projecting results in a morphology model of the whole fruit. The result is a synthetic representation of cell morphology variations within the whole fruit. The approach is generic and can be adapted to a wide range of products, as well as for images obtained from different acquisition modalities.

We used the tomato pericarp as a model for fleshy fruits. Two different scales were investigated: 3D confocal microscopy, and macroscopy imaging of pericarp slices. The morphology of the tomato pericarp from 3D microscopy images was assessed through the surface area of cell walls, taking into account the sampling probabilities of the 3D voxels. The morphology of macroscopy images was assessed through greyscale granulometry using tools from mathematical morphology. Spatial variations within pericarp was described by computing estimates for 10 classes of geodesic distances, and 20 classes of depth within pericarp, for each characterisation method.

2 Material and Methods

2.1 Fruit Sampling

Tomatoes of the Tradiro variety were provided by the CTIFL (French Interprofessional and Technical Centre for Fruits and Vegetables) and stored at 20°C in a dark room. Fourteen fruits at mature green or breaker stage and approximately the same size were used to establish the cartography.

Ten sampling regions were considered, equally spaced between the pedicel scar and the apical region of the tomato (Figure 1). For each tomato, five sampling points in five different regions were chosen. The longitudinal position of the sampling points was chosen uniformly.

For each sampling region, a pericarp cylinder was extracted perpendicular to the surface, using a core-borer. Sections (200-µm thick) of fresh tissue perpendicular to the epidermis were obtained using a vibrating blade microtome.

2.2 Imaging of the whole fruit

After sampling, each tomato was divided into several quarters. Colour images of one side of each quarter were acquired using a flat scanner. The contour was extracted and the two points corresponding to the pedicel scar and the tomato apex were manually selected.

An average contour was computed for each of the 14 tomato fruits by polynomial fitting. An average contour was assessed to obtain a global model fruit for the Tradiro variety. This average contour was used to visualise a 3D global fruit morphology as the revolution surface of the average contour and as the reference template to represent the cartography of cell morphology (Legland et al, 2012).

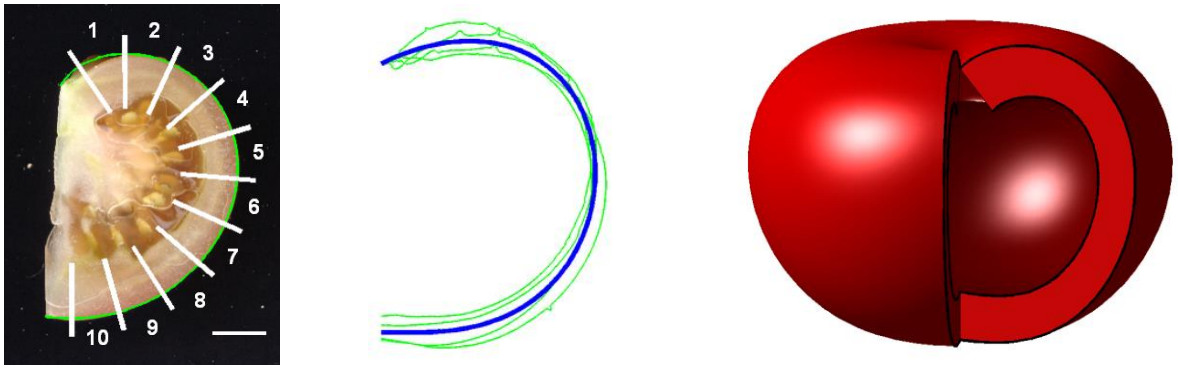

Fig. 1 Left: representation of the ten sampling regions used in this study. Middle: modelling of an average contour by polynomial fitting of several discretised contours. Right: 3D representation of the average tomato model.

2.3 Macroscopy imaging

Images of pericarp sections were acquired using a prototype of the macrovision system specifically built to observe plant tissues (mostly fruits, stems and roots) without any staining step (Devaux et al., 2009). The system, known as "BlueBox", includes a CCD camera equipped with a lens corresponding to a 0.6 X magnification. An optical fibre ring is placed on a dark background in order to backlight sections at an angle of around 35°, and samples are placed in a 5-cm Petri box over the ring. Under this configuration, light is sent at oblique angles to the sample, providing a dark-field illumination. The camera and lens were set to observe a 11.3 mm × 8.5 mm field of view. Images were digitised as matrices of 1620 × 1220 pixels of 6.98 × 6.98 µm.

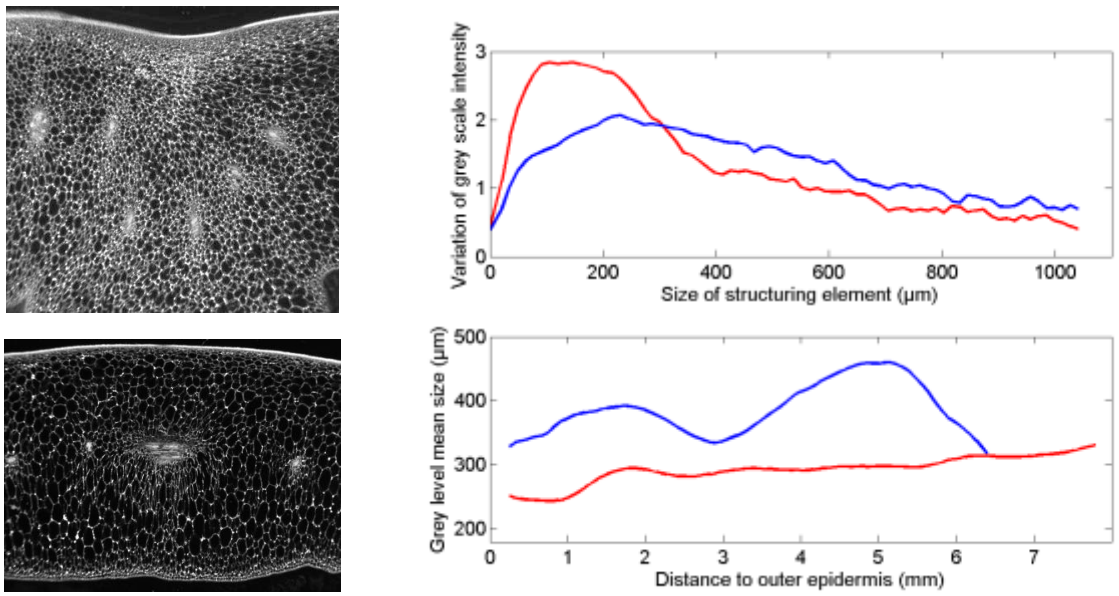

Fig. 2 Left: two sample slices of the same tomato sampled close to the pedicel and in the equatorial region, observed using macroscopy. Top right: global granulometric curves obtained from each image. Bottom right: profiles of average grey level mean size as a function of the distance to the epidermis.

Image texture analysis derived from mathematical morphology (Soille, 2003) was used to quantify cell size from macroscopic images (Devaux, 2008). Grey level granulometry was first applied on regions of interest corresponding to the whole pericarp. Figure 2 shows granulometric curves computed on two sample slices. showing a peak around 150 micron for the image close to the pedicel, and a larger peak around 300 microns for the image in the equatorial region.

In order to compare granulometric curves for a set of samples, curves were summarised by computing grey level mean sizes corresponding to geometric mean of the granulometric curves (Legland et al., 2012). Gray level mean sizes can be integrated over sampling regions to depict profile of morphology depending on geodesic distance to the pedicel. Using vertical or horizontal linear structuring elements, it is possible to assess the grey level mean size in the radial or tangential direction (Legland et al, 2012). The radial direction was considered here.

The grey level mean sizes can be measured for different regions of interest within a single image. By considering regions of interest corresponding to different classes of distances to the outer epidermis, it is possible to compute a profile of grey level mean size variation with the distance to epidermis (Figure 2). The image close to the pedicel is composed of small cells in all positions, whereas the grey level mean size in equatorial slice varies according to the position: smaller cells are located close to the epidermises, and around vascular bundles.

2.4 3D confocal microscopy imaging

Pericarp sections were stained using acridin orange. Images were acquired with a Zeiss LSM410 confocal laser scanning microscope, using a ×10 air immersion lens with a numerical aperture of 0.5. The z-scanning step was set to 4 µm in accordance with the optical section thickness. The excitation wavelength was 488 nm and the light emitted over 515 nm was collected using a long-pass filter. Each image was digitised as a 512 × 512 pixel matrix with grey levels coded between 0 (black) and 255 (white). The size of the voxels was 2.5 µm in the x and y directions, resulting in a 1.275 × 1.275 mm^2 field of view. The sets of optical sections were considered as 3D image stacks of 512 × 512 × Nz voxels, with Nz being the number of sections.

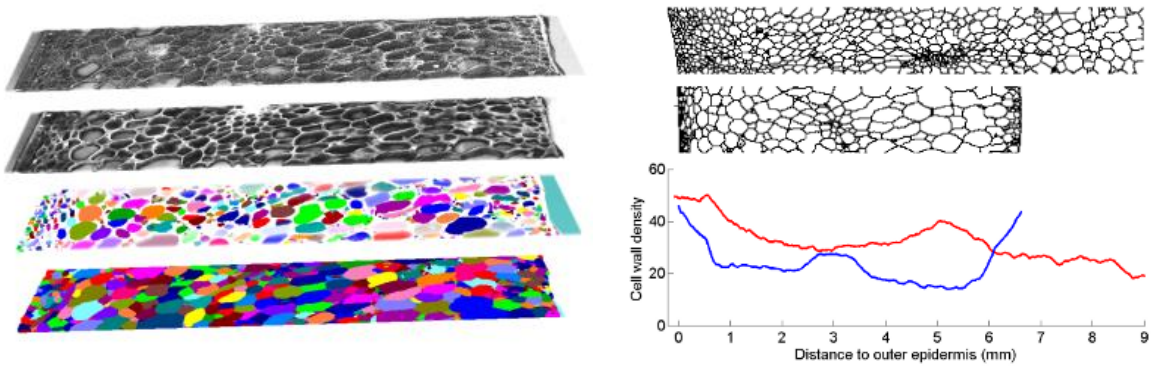

Fig. 3 Several steps of image processing and analysis. Left, from top to bottom: original 3D image, image enhanced using directional filtering, detection of 3D markers, segmentation using 3D watershed. Right: two sample slices sampled in two regions of the same tomato, and the profiles of cell wall surface density depending on the distance to epidermis.

In order to enhance cell walls, images were filtered using directional median filtering (Soille, 2003; Legland et al., 2009). Several median filters were applied, using line segments (length = 25 pixels) with 16 different orientations as structuring elements. The maximum value over orientations was kept as final value. Cellular spaces were segmented by applying a constrained watershed (Soille, 2003; Legland et al., 2009). The extended minima (threshold = 10) were used as markers of cells and intercellular spaces.

The thickness of 3D mosaic images was varying between 30 and 60 microns, whereas tomato cells can be as large as 1 mm (Devaux et al, 2008). Consequently, most of the cells could not be entirely observed. Cellular morphology at the microscopic scale can be described by the cell wall surface area density, defined as the ratio of cell wall surface area over the volume of pericarp. Since more cell walls are observed in the presence of small cells, cell wall surface density can be related to cell size. Cell wall surface area was measured using local voxel configuration counts (Legland et al., 2007), and weighted by local sampling probability as described in Legland et al. (2008, 2012).

3 Results

3.1 Global morphology

Results obtained from each individual image were pooled to assess the global morphology of the Tradiro variety. Using macroscopy, the average grey level mean size was equal to 358 µm (± 3 µm). Using confocal microscopy, pericarp volume estimate was equal to 88.7 cm^3 (± 0.8 cm^3), and cell wall surface area estimate was equal to 2.41 m^2 (± 0.81 m^2), resulting in a final estimate of cell wall surface density equal to 26.94 mm^2/mm^3 (± 0.59 mm^2/mm^3). With an assumption of pericarp composed of spherical cells of equal radius, this corresponds to an average cell diameter of 277 µm. The results obtained at the two scales present large differences. A first interpretation is that greyscale granulometry is an indirect method that overestimates cell size, whereas cell wall surface area estimation from 3D confocal images tend to detect more small cells, resulting in a smaller cell size.

3.2 Cell morphology profiles

Two profiles of cell morphology can be computed from each imaging scales. Profiles of grey level mean size or of cell wall surface density can be normalised to relative distance between outer and inner epidermis, revealing that cells are smaller close to the pericarp epidermises and around vascular bundles (Figure 4). Average grey level mean size or cell wall surface area density can also be computed for different sampling regions, thus describing the variations of cell morphology as a function of the distance to the cuticle (Figure 4). In particular, cells appear to be smaller close to the pedicel and close to the apex of the tomato.

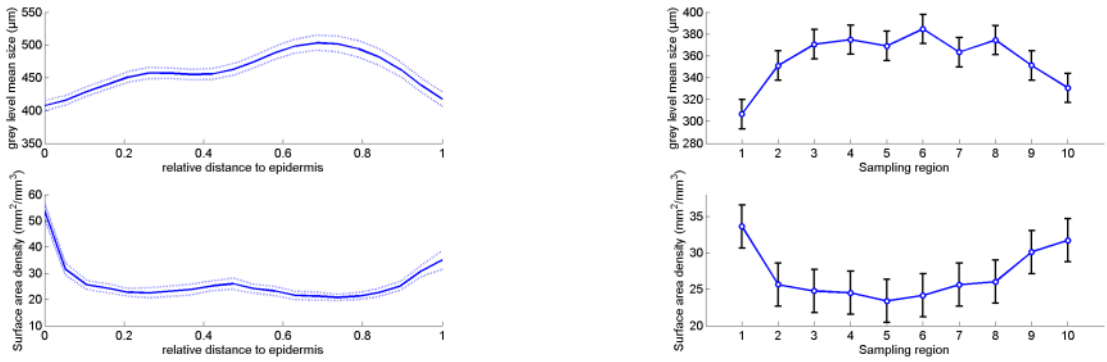

Fig. 4 Profiles of cell morphology variation depending on the distance to epidermis (left) or on the sampling region (right), using macroscopy imaging (top) or 3D confocal imaging (bottom).

3.3 Cell morphology cartographies

By combining the localisation of measurements both as a function of the relative distance to the epidermises and to the pedicel, it is possible to compute a statistical cartography of the cell morphology within the whole fruit (Figure 5). Grey level granulometry from macroscopy images reveals that large cells are located mostly in the inner part of the equatorial pericarp. Symmetrically, cell wall surface area estimates obtained from 3D confocal microscopy shows that cell walls are more numerous around epidermises, and close to the apices of the pericarp.

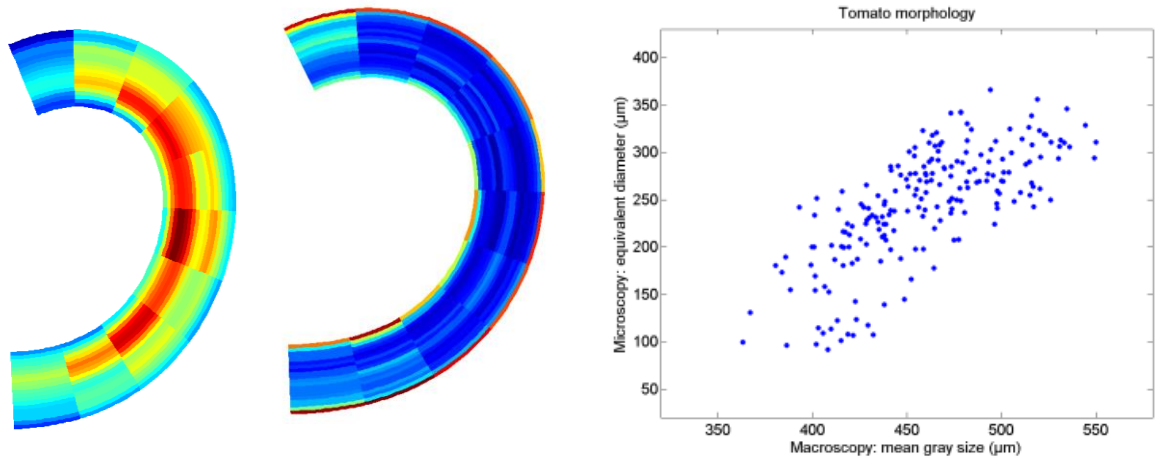

Fig. 5 Statistical cartographies of cell morphology obtained from macroscopy imaging (left), from 3D confocal microscopy (centre), and comparison of the cell diameters computed from each observation scale.

The measurements obtained from both imaging scales can be related each other. By computing average cell diameter in each region of the resulting cartographies, a correlation coefficient of around 0.75 can be obtained. The cell size obtained from macroscopy is much larger than the one obtained from microscopy, showing a fractal effect: the measured size depends on the resolution of the measurement device (Mandelbrot, 1967).

4 Conclusions

Cell morphology observed at microscopic or macroscopic scale could be related to observations of tissue within the whole fruit, e.g., using magnetic resonance imaging or tomography (Mebatsion et al., 2009; Musse et al., 2010). The cartographies obtained from acquisitions at different observation scales could be combined and compared, envisioning the foundation of a multi-modal atlas of cell morphology within the whole fruit.

Acknowledgements

The authors thank the CTIFL for providing the samples used in this study. This work was supported by the Sixth Framework Program of the European Union through the EU-SOL Project.

References

Cheniclet, C., Rong, W.Y., Causse, M., Frangne, N., Bolling, L., Cade, J.P. and Renaudin, J.-P., 2005. Cell expansion and endoreduplication show a large genetic variablilty in pericarp and contribute strongly to tomato fruit growth. Plant Physiol. 139, 1984–1994.

Devaux, M.-F., Bouchet, B., Legland, D., Guillon, F., Lahaye, M., 2008. Macro-vision and grey level granulometry for quantification of tomato pericarp structure. Postharvest Biol. Technol. 47, 199–209.

Devaux, M.-F., Sire, A. and Papineau, P., 2009. Macrovision et analyse granulométrique en niveau de gris pour l'analyse histologique de tissus végétaux. Cahiers techniques de l'INRA, numéro spécial imagerie: 93–100

Gray, J.D., Kolesik, P., Hoj, P.B. and Coombe, B.G., 1999. Confocal measurement of the three-dimensional size and shape of plant parenchyma cells in a developing fruit tissue. Plant Journal 19, 229–236.

Ho, Q.T., Verboven, P., Verlinden, B.E., Schenk, A., Delele, M.A., Rolletschek, H., Vercammen, J., Nicolaï, B.M., 2010. Genotype effects on internal gas gradients in apple fruit. J. Exp. Bot. 61, 2745–2755.

Legland, D., Kiêu, K. and Devaux, M.-F., 2007. Computation of Minkowski measures on 2D and 3D binary images. Image Anal. Stereol. 26, 83–92.

Legland, D., Devaux, M.-F., Kiêu, K. and Bouchet, B., 2008. Stereological estimation for layered structures based on slabs perpendicular to a surface. J. Miscrosc. 232, 44–55.

Legland, D. and Devaux, M.-F., 2009. Détection semi-automatique de cellules de fruits charnus observés par microscopie confocale 2D et 3D. Cahiers techniques de l'INRA. Special issue on imagery, 7–16

Legland, D., Guillon, F., Kiêu, K., Bouchet, B. and Devaux, M.-F., 2010. Stereological estimation of cell wall density of DR12 tomato mutant using 3D confocal imaging. Ann. Bot. 105 (2), 265–276.

Legland, D., Devaux, M.-F., Bouchet, B., Guillon, F., Lahaye, M., 2012. Cartography of cell morphology in tomato pericarp at the fruit scale. J. Miscrosc. 247, 78–93.

Mandelbrot, B., 1967. How Long Is the Coast of Britain? Statistical Self-Similarity and Fractional Dimension. Science, New Series 156(3775), 636–638.

Mebatsion, H.K., Verboven, P., Ho, Q.T., Verlinden, B.E., Nicolaï, B.M., 2008. Modelling fruit (micro)structures, why and how? Trends Food Science Technol. 19, 59–66.

Mebatsion, H.K., Verboven, P., Melese Endalewa, A., Billen, J., Ho, Q.T. and Nicolaï, B.M., 2009. A novel method for 3-D microstructure modeling of pome fruit tissue using synchrotron radiation tomography images. J. Food Eng. 93(2), 141–148.

Musse, M., De guio, F., Quellec, Q., Cambert, M., Challois, S. and Davenel, A. (2010) Quantification of microporosity in fruit by MRI at various magnetic fileds: comparison with X-ray microtomography. Magnetic Resonance Imaging 28, 1525-1534.

Pieczywek, P.M., Zdunek, A., 2012. Automatic classification of cells and intercellular spaces of apple tissue. Computers and Electronics in Agriculture 81, 72–78.

Schotsmans, W., Verlinden, B.E., Lammertyn, J., Nicolaï, B.M., 2004. The relationship between gas transport properties and the histology of apple. J. Sci. Food Agric. 84, 1131–1140.

Soille, P., 2003. Morphological Image Analysis, Springer.